Decay Pattern of Pygmy States Observed in Neutron-Rich ^{26}Ne

J. Gibelin,[1,2,*] D. Beaumel,[1] T. Motobayashi,[3] Y. Blumenfeld,[1] N. Aoi,[3] H. Baba,[3] Z. Elekes,[4] S. Fortier,[1] N. Frascaria,[1] N. Fukuda,[3] T. Gomi,[3] K. Ishikawa,[5] Y. Kondo,[5] T. Kubo,[3] V. Lima,[1] T. Nakamura,[5] A. Saito,[6] Y. Satou,[5] J.-A. Scarpaci,[1] E. Takeshita,[2] S. Takeuchi,[3] T. Teranishi,[7] Y. Togano,[2] A. M. Vinodkumar,[5] Y. Yanagisawa,[3] and K. Yoshida[3]

[1]*Institut de Physique Nucléaire, IN_2P_3-CNRS, Université Paris Sud, F-91406 Orsay, France*
[2]*Department of Physics, Rikkyo University, 3-34-1 Nishi-Ikebukuro, Toshima, Tokyo 171-8501, Japan*
[3]*RIKEN (The Institute of Physical and Chemical Research), 2-1 Hirosawa, Wako, Saitama 351-0198, Japan*
[4]*Institute of Nuclear Research of the Hungarian Academy of Sciences, PO Box 51, H-4001 Debrecen, Hungary*
[5]*Department of Physics, Tokyo Institute of Technology, Tokyo 152-8551, Japan*
[6]*Center for Nuclear Study, University of Tokyo, RIKEN Campus, 2-1 Hirosawa, Wako, Saitama 351-0198, Japan*
[7]*Department of Physics, Kyushu University, 6-10-1 Hakozaki, Higashi, Fukuoka 812-8581, Japan*

(Received 7 March 2008; published 19 November 2008)

Coulomb excitation of the exotic neutron-rich nucleus ^{26}Ne on a ^{208}Pb target was measured at 58 MeV/u in order to search for low-lying $E1$ strength above the neutron emission threshold. This radioactive beam experiment was carried out at the RIKEN Accelerator Research Facility. Using the invariant mass method in the $^{25}\mathrm{Ne} + n$ channel, we observe a sizable amount of $E1$ strength between 6 and 10 MeV excitation energy. By performing a multipole decomposition of the differential cross section, a reduced dipole transition probability of $B(E1) = 0.49 \pm 0.16e^2$ fm^2 is deduced, corresponding to $4.9 \pm 1.6\%$ of the Thomas-Reiche-Kuhn sum rule. For the first time, the decay pattern of low-lying strength in a neutron-rich nucleus is measured. The extracted decay pattern is not consistent with several mean-field theory descriptions of the pygmy states.

DOI: 10.1103/PhysRevLett.101.212503 PACS numbers: 24.30.Gd, 24.30.Cz, 25.70.De

The advent of beams of atomic nuclei with large neutron/proton ratios has offered the possibility to investigate new phenomena associated with the excess of neutrons. An often quoted property of such exotic nuclei is the halo effect, an abnormal extension of matter distribution observed for the first time in light neutron-rich isotopes in the mid 1980s [1]. Beyond static properties, the question of the occurrence of new dynamical modes associated with the excess neutrons has been investigated both theoretically and experimentally. Predictions were given in the early 1990s in favor of such modes [2,3]. In these calculations, the dipole response of neutron-rich (n-rich) nuclei exhibits a small component at energies lower than the standard giant dipole resonance, often depicted as the oscillation of a deeply bound core against a neutron halo or skin, giving rise to a so-called pygmy resonance. Such modifications of the response function of nuclei have direct implications for astrophysics. The strong influence of an—even small—percentage of $E1$ strength located above particle threshold on neutron capture reactions has been studied in [4]. More recently, the link between pygmy dipole strength, neutron skin thickness and symmetry energy in asymmetric nuclear matter, which has a strong impact on several neutron-star properties has been stressed [5]. Experimentally, the presence of low-lying dipole strength exhausting a sizable amount of the Thomas-Reiche-Kuhn (TRK) energy weighted sum rule in n-rich nuclei is now established. It was first revealed in light dripline nuclei in breakup reactions using high-Z targets [6]. Later on, the nonresonant nature of the dipole strength found in some light n-rich nuclei such as ^{11}Be was stated [7]. In heavier nuclei, low-lying dipole strength has been recently observed in Coulomb breakup experiments at high energy performed at the GSI facility, Darmstadt, on oxygen [8] and tin [9] isotopes. In the latter case, an amount of nearly 5% of the TRK sum rule has been measured at around 10 MeV excitation energy in ^{130,132}Sn nuclei, in agreement with several mean-field models. Interestingly, conflicting interpretations are provided by the quoted models concerning the microscopic structure of these states. Within the relativistic quasiparticle random phase approximation (QRPA) calculations [10], relatively collective pygmy states are predicted, while nonrelativistic QRPA including phonon coupling involves essentially individual transitions [11]. No conclusion can be brought on the microscopic structure of these states in the absence of observables other than the strength distribution. Both approaches nevertheless agree that the excitations are driven by the excess neutrons.

In the present Letter we investigate low-lying dipole strength in the ^{26}Ne isotope for which an important redistribution of dipole strength as compared to the stable ^{20}Ne is predicted by Cao and Ma [12]. In this calculation, almost 5% of the TRK sum rule is exhausted by a structure centered around 8.5 MeV. This region in energy is located between the one-neutron and the two-neutron emission threshold. We performed a Coulomb excitation experiment by bombarding a lead target by ^{26}Ne at intermediate en-

ergy, and used the invariant mass method to reconstruct the $B(E1)$ strength from the $^{26}\mathrm{Ne} \rightarrow {}^{25}\mathrm{Ne} + n$ channel. After determining the strength distribution, we extract for the first time neutron branching ratios of the populated pygmy states to levels in the daughter nucleus (^{25}Ne). These observables provide detailed insight on the microscopic structure of the populated states, as long as the observed decay mode is not statistical [13].

The experiment was performed at the RIKEN Accelerator Research Facility. A secondary ^{26}Ne beam was produced through fragmentation of a 95 MeV/u, 60 pnA ^{40}Ar primary beam on a 2-mm-thick ^{9}Be target. The ^{26}Ne fragments were separated by the RIKEN Projectile Fragment Separator (RIPS) [14]. Beam particle identification was unambiguously performed by means of the time-of-flight (TOF) between the production target and the second focal plane. The 80% pure ^{26}Ne beam of intensity $\sim 5 \times 10^3$ pps and incident energy 58 MeV/u, was tracked with two parallel-plate avalanche counters providing incident angle and hit position on the reaction targets (alternatively 230 mg/cm^2 $^{\mathrm{nat}}$Pb and 130 mg/cm^2 ^{27}Al). Data obtained with the ^{27}Al target are used in the following to estimate the contribution of nuclear excitation to the data.

The outgoing charged fragments were detected using a set of telescopes placed at 1.2 m downstream of the target. They consisted of two layers (X and Y) of 500 μm single-sided silicon strip detectors with 5 mm strips which yielded an energy-loss resolution for neon isotopes of 1.5 MeV (FWHM). An additional layer used 3 mm-thick Si(Li) detectors made at the Institut de Physique Nucléaire d'Orsay. The resolution on the remaining energy (E) was 9 MeV (FWHM). Unambiguous mass and charge identification of all projectilelike fragments was obtained using the $E - \Delta E$ method.

In-beam gamma rays were detected using the 4π gamma array DALI2 [15], which consists of 152 NaI(Tl) detectors placed around the target. For 1.3 MeV gamma rays, the measured efficiency is approximately 15% and the energy resolution is 7% (FWHM). The Doppler corrected gamma energy distribution obtained in coincidence with the ^{25}Ne isotope allows us to identify the gamma decay from the adopted 1702.7(7), 2030(50), and 3316.4(11) keV excited states.

The hodoscope for neutron detection was an array of 4 layers of 29 plastic rods each, placed 3.5 m downstream of the target. The total intrinsic efficiency for the detection of 60 MeV neutrons was calculated to be 25% [16]. Finally, 29 thin plastic scintillators covered the front face of the wall in order to veto charged particles as well as to provide an active beam stopper. The neutron position was determined with an error of ± 3 cm and the energy, from TOF information, with a 2.5 MeV (FWHM) resolution for the neutrons of interest.

A simulation of the experimental setup using the Geant 3 package [17] was performed in order to correct the data for the experimental acceptance. Using this simulation, the angular distribution for elastic scattering of ^{26}Ne on $^{\mathrm{nat}}$Pb at 55 MeV/u was obtained and compared with optical model calculations based on an optical potential for the $^{20}\mathrm{Ne} + {}^{\mathrm{nat}}\mathrm{Pb}$ system at 40 MeV/u [18]. Another check for both the simulation and the optical potential used was provided by the ^{26}Ne $B(E2; 0_1^+ \rightarrow 2_1^+)$ [19], extracted by comparing the shape and the amplitude of the angular distribution of the experimental inelastic scattering with the corresponding theoretical calculation. For the $^{26}\mathrm{Ne} + {}^{27}\mathrm{Al}$ reaction, we empirically generated optical potential parameters [20] and compared the result with the experimental elastic scattering.

Using the invariant mass method, the excitation energy of an unbound state in the ^{A}X nucleus decaying to a state in ^{A-1}X can be expressed by: $E^* = E_{\mathrm{rel}} + S_n + \sum_i E_{\gamma_i}$, where E_{rel} is the relative energy between the neutron and the fragment ^{A-1}X, S_n the one-neutron emission threshold, and $\sum_i E_i$ the summed energy of the gammas involved in the subsequent decay of the daughter nucleus ^{A-1}X. The gamma detection efficiency was not high enough to perform an event-by-event gamma calorimetry. Hence, our reconstruction technique took into account independently the population of every state of the ^{A-1}X daughter nucleus [20,21]. This method has been successfully tested on simulations. We also included the detector resolutions and hence estimated the excitation energy resolution to be 0.8 MeV at $E^* = 8$ MeV.

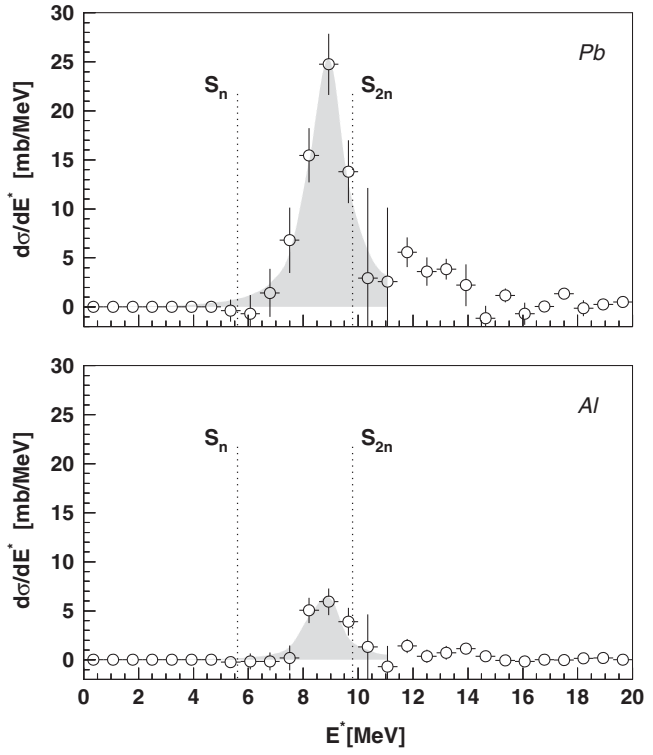

FIG. 1. Top: Excitation energy distribution in ^{26}Ne reconstructed from the $^{25}\mathrm{Ne} + n$ decay channel with $^{\mathrm{nat}}$Pb target. The shaded area is a tentative Lorentzian fit. Bottom: Same as previous but for the ^{27}Al target.

The excitation energy spectra reconstructed for the $^{25}\mathrm{Ne} + n$ decay channel obtained with the Pb and Al targets are represented in Fig. 1. Above 10 MeV, the decay of ^{26}Ne is expected to occur mainly by 2-neutron emission. Between 8 and 10 MeV, a sizable amount of cross section is observed for both targets. In intermediate energy inelastic scattering with a heavy target such as Pb, the spectrum is dominated by Coulomb excitation of $E1$ states. Conversely, the dipole excitation is relatively low with a light target such as Al. The contribution of possible $E2$ excitation to the spectrum obtained with the lead target has been determined by using data taken with the aluminum target and the coupled channels ECIS97 code [22]. Assuming a simple collective vibrational mode with equal nuclear and Coulomb deformation lengths, the $E2$ nuclear and Coulomb deformation parameters were extracted from the measured cross section with the Al target ($\sigma_{\mathrm{Al}} = 9.1 \pm 2.3$ mb). The corresponding $L = 2$ cross section in lead was then calculated using the deformation lengths extracted in the previous step. After subtraction of this $E2$ contribution, the resulting $\sigma_{\mathrm{Pb}}^{L=1} = 48.5 \pm 4.8$ mb cross section corresponds to a Coulomb deformation parameter $\beta_{\mathrm{C}} = 0.087 \pm 0.008$ which leads to $B(E1) = 0.55 \pm 0.05e^2$ fm^2 *via* the following relation with the Coulomb radius R_C: $B(E1; 0^+ \rightarrow 1^-) = (\frac{3}{4\pi} Z_p e R_C \beta_C^{L=1})^2$, where Z_p is the projectile proton number. This value of reduced transition probability corresponds to $5.5 \pm 0.6\%$ of the TRK sum rule for an excitation energy of 9 MeV.

The high granularity of the present setup, allows to reconstruct the scattering angular distribution for ^{26}Ne on the $^{\mathrm{nat}}$Pb target (Fig. 2) and to extract the $E1$ excitation by means of a multipole decomposition analysis. The $L = 1$ and $L = 2$ angular distributions (dotted and dashed lines) were obtained from simulations based on ECIS97 angular distribution calculated for $E^* = 9$ MeV. The data were fitted with a linear combination of the two distributions since $L = 2$ and $L > 2$ distributions were found to exhibit similar shapes. The result of the fit gives $B(E1) = 0.49 \pm 0.16e^2$ fm^2 which corresponds to $4.9 \pm 1.6\%$ of the TRK sum rule around 9 MeV excitation energy. Assuming that the remaining part of the contribution is due to $L = 2$ excitation, we obtain $B(E2\uparrow) = 49 \pm 8e^2$ fm^4. The two methods to extract the $E1$ component thus provide very consistent results. A third method presented in [20] also leads to the same conclusion. This shows that, within the error bars, possible contribution of modes such as isoscalar $L = 1$ states to the data taken with the Al target does not affect the final result on $B(E1)$.

Theoretical calculations have been performed within various frameworks. Using the relativistic QRPA (RQRPA) and the response function formalism, Cao and Ma [12] predict an $E1$ pygmy state centered around 8.4 MeV and exhausting 4.5% of the TRK sum rule, close to our experimental values. RQRPA calculations for axially deformed nuclei also report a pygmy state below 10 MeV excitation energy [23]. No corresponding percentage of TRK sum rule is reported. Similarly, a redistribution of the strength with a peak at low energy is also predicted by (nonrelativistic) deformed QRPA calculations using Gogny forces [24] and Skyrme forces [25]. All these calculations agree on the presence of a structure at low excitation energy in the $E1$ response function. In order to get deeper insight into the microscopic structure of these states, one can examine the dominant configurations involved, which can be extracted from the calculations of Refs. [23–25] performed in the matrix formalism. In the first two calculations, the dominant transitions are found to be $2s_{1/2} \rightarrow 2p_{3/2}$ and/or $2s_{1/2} \rightarrow 2p_{1/2}$, corresponding to the promotion of neutrons essentially from the last occupied orbit of ^{26}Ne to fp shells.

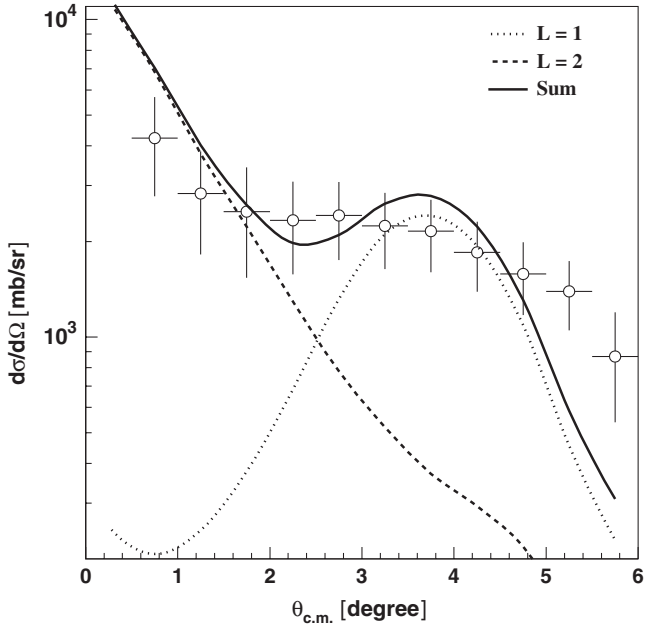

FIG. 2. Result (solid line) of the multipole decomposition of the experimental differential cross section of the structure at $E^* \sim 9$ MeV excited in ^{26}Ne using the lead target, and contributions of $L = 1$ (dotted line) and $L = 2$ (dashed line) multipoles.

It is well known that the decay pattern of continuum states can give access to the components of the wave function of these states. The excitation energy reconstruction method used in the present experiment [20] allows us to extract for the first time data on the decay of pygmy resonances of neutron-rich nuclei. The experimental branching ratios to bound states of ^{25}Ne are presented in Table I. For both Pb and Al targets, the branching ratio for the decay to the ground state (GS) of ^{25}Ne is compatible with zero. By using the simulation code, it was checked that any decay pattern including a sizable branch to the GS is incompatible with the experimental results. The large difference between branching ratios obtained with the two targets proves that states of different nature have been excited. We then deduced the $L = 1$ and $L = 2$ components on the Pb target by assuming that the Al target

TABLE I. Experimental neutron branching ratios for the structure at $E^* \sim 9$ MeV in ^{26}Ne to the ^{25}Ne states, compared to statistical decay calculations [26] for several multipolarities. We assumed that the reaction on ^{27}Al induces only $L = 2$ transitions, see text.

Final ^{25}Ne state		Experiment			Statistical decay		
Energy (MeV)	J^π	Pb	Pb ($L = 1$)	Pb ($L = 2$) = Al	$L = 1$	$L = 2$	$L = 3$
0.0	$1/2^+$	5^{+17}_{-5}%	5^{+32}_{-5}%	4^{+5}_{-4}%	40%	28%	22%
1.7 & 2.0	$5/2^+ + 3/2^+$	66% ± 15%	42% ± 30%	95^{+5}_{-15}%	55%	67%	75%
3.3	$(3/2^-)$	35% ± 9%	60% ± 17%	5^{+6}_{-5}%	5%	4%	3%

induces only a $L \geq 2$ excitation, as described above. For comparison, we performed a statistical decay calculation assuming $L = 1, 2, 3$ emitting states using the CASCADE code [26], spins and parities of populated states in ^{25}Ne being those listed in Table I. The decay is not statistical, as observed in light nuclei [13]. Since the GS of ^{25}Ne has $J^\pi = 1/2^+$, the decay to this state becomes weaker with increasing spin of the emitting state due to penetrability effects.

A striking feature of the observed decay pattern is the absence of decay to the ^{25}Ne GS, which is in contradiction with the predicted structure of the pygmy states. Indeed, it is established that the ^{25}Ne GS configuration mainly corresponds to a neutron in the $2s_{1/2}$ orbit, the experimental spectroscopic factor obtained from the ^{24}Ne(d, p) reaction being 0.8 [27]. If the main configuration of the pygmy state were actually $\nu(2s^{-1}_{1/2}2p_{3/2})$ or $\nu(2s^{-1}_{1/2}2p_{1/2})$ a strong decay to the ^{25}Ne GS should occur, even favored by penetrabilities. This discrepancy indicates that the populated pygmy states are more mixed and/or involve different transitions. Interestingly, calculations reported in [23] predict a dominant contribution of the $K^\pi = 1^-$ state, with nearly equal weights of $\nu(2s^{-1}_{1/2}2p_{1/2})$ and $\nu(1d^{-1}_{5/2}1f_{7/2})$ transitions which is in better qualitative agreement with our data.

Theoretical branching ratios, presently not available, are highly desirable for a more precise comparison. We note that they could also be obtained from shell-model calculations by combining the single-particle spectroscopic factors and penetrability coefficients.

In summary the present study of the neutron-rich nucleus ^{26}Ne using intermediate energy inelastic scattering has shown the presence of pygmy states located around 9 MeV excitation energy. The contribution of $E1$ states corresponds to nearly 5% of the TRK sum rule. These global features are in agreement with self consistent mean-field calculations performed in various frameworks. The decay pattern of the observed pygmy states has been measured for the first time, providing a stringent test of the microscopic models describing the wave function of these states. The measured decay pattern is not consistent with models predicting a structure corresponding to excitations of neutrons from the Fermi surface. Making use of the new facilities RIBF (Radioactive Ion Beam Facility) and Big RIPS, future studies will investigate nuclei located even further from stability.

*Present address: LPC Caen, Université de Caen, F-14050 Caen Cedex, France.
gibelin@lpccaen.in2p3.fr

[1] I. Tanihata *et al.*, Phys. Rev. Lett. **55**, 2676 (1985).
[2] Y. Suzuki *et al.*, Prog. Theor. Phys. **83**, 180 (1990).
[3] P. Van Isacker, M. A. Nagarajan, and D. D. Warner, Phys. Rev. C **45**, R13 (1992).
[4] S. Goriely *et al.*, Nucl. Phys. A **739**, 331 (2004).
[5] A. Klimkiewicz *et al.*, Phys. Rev. C **76**, 051603(R) (2007).
[6] I. Tanihata, Prog. Part. Nucl. Phys. **35**, 505 (1995), and references therein.
[7] N. Fukuda *et al.*, Phys. Rev. C **70**, 054606 (2004).
[8] A. Leistenschneider *et al.*, Phys. Rev. Lett. **86**, 5442 (2001).
[9] P. Adrich *et al.*, Phys. Rev. Lett. **95**, 132501 (2005).
[10] N. Paar, P. Ring, T. Niksic, and D. Vretenar, Phys. Rev. C **67**, 034312 (2003).
[11] D. Sarchi *et al.*, Phys. Lett. B **601**, 27 (2004).
[12] L.-G. Cao and Z.-Y. Ma, Phys. Rev. C **71**, 034305 (2005).
[13] M. N. Harakeh and A. van der Woude, *Giant Resonances: Fundamental High-Frequency Modes of Nuclear Excitation* (Oxford University Press, New York, 2001).
[14] T. Kubo *et al.*, Nucl. Instrum. Methods Phys. Res., Sect. B **70**, 309 (1992).
[15] S. Takeuchi *et al.*, RIKEN Accel. Prog. Rep. **36**, 148 (2002).
[16] N. Fukuda, Ph.D. thesis, University of Tokyo, 2004, and references therein.
[17] R. Brun *et al.*, CERN Report No. CERN DD/EE/84-1, 1986.
[18] T. Suomijarvi *et al.*, Nucl. Phys. A **491**, 314 (1989).
[19] J. Gibelin *et al.*, Phys. Rev. C **75**, 057306 (2007).
[20] J. Gibelin, Ph.D. thesis, Paris XI University, 2005; http://hal.in2p3.fr/docs/00/05/88/11/PDF/thesis_gibelin.pdf.
[21] J. Gibelin *et al.*, Nucl. Phys. A **788**, 153c (2007).
[22] J. Raynal (unpublished).
[23] D. Arteaga and P. Ring, Prog. Part. Nucl. Phys. **59**, 314 (2007), and private communication.
[24] S. Peru *et al.*, Nucl. Phys. A **788**, 44 (2007).
[25] K. Yoshida and N. V. Giai, Phys. Rev. C **78**, 014305 (2008).
[26] F. Puhlhofer, Nucl. Phys. A **280**, 267 (1977).
[27] B. Fernandez-Dominguez *et al.*, Prog. Part. Nucl. Phys. **59**, 389 (2007).